Micro-Vibration Attenuation Using Novel Flexible Pivot Design

Luc Blecha*, Yoël Puyol*, Simon Hayoz*, Martin Humphries** and Fabrice Rottmeier*

Abstract

Flexible pivots present numerous advantages such as no wear, no particle generation and predictable torque. In addition, the patented design presented in this paper adds high stiffness tunability, large angle, nearly constant radial stiffness over the entire range of motion, and infinite life capability. A design optimization software has been developed to generate within a few hours custom flexible pivot designs matching specific application requirements such as pivot angle, torsional, radial, axial, bending stiffness, maximal stress, and buckling factors. The flexible pivot design is an enabling technology for many applications and in particular for ultra-stable pointing mechanisms. A novel concept of an ultra-stable pointing mechanism using a flexible pivot is presented. It is shown with a simple Nastran model that the micro-vibration impact on pointing mirror stability can be theoretically decreased by 3 to 8 orders of magnitude in the 50-200 Hz frequency range, and by more than 9 orders of magnitude above 200 Hz in comparison with a design using ball bearings. The achieved pointing accuracy makes the need of a fine pointing mechanism unnecessary. The total mass, volume and costs can thus be drastically reduced in comparison to the existing solution today on the market that uses coarse and fine pointing mechanisms. A fully functional and motorized breadboard has been built and showed full hemispherical pointing range.

Large-Angle Flexible Pivot Design

The principle of the Large-Angle Flexible Pivot is based on controlled deformation of structures in pure bending within their elastic limit. The flexible pivot consists of two interface rings connected by flexible elements (Figure 1). The first ring is the stator and the second is the rotor. A first set of flexible elements connect the stator ring to a central cylinder. These spokes are composed of a thin elongated blade connected to another smaller blade called T-bars as they are forming a T-shape. The T-bars are connected to the stator. From the central cylinder, connecting members connect the first central cylinder to an outer ring by means of another set of T-bars. From the outer ring, the structure is symmetrical. The outer ring is thus connected to another central ring on the rotor side by connecting members and T-bars. Finally, the second central ring is connected to the rotor ring by a set of spokes and a fourth set of T-bars. This is a so-called two-stage design that can achieve a rotation of ±70° for infinite life conditions and higher angular range with reduced life.

* Almatech SA, Lausanne, Switzerland; luc.blecha@almatech.ch

** SpaceMech Ltd., Bristol, UK

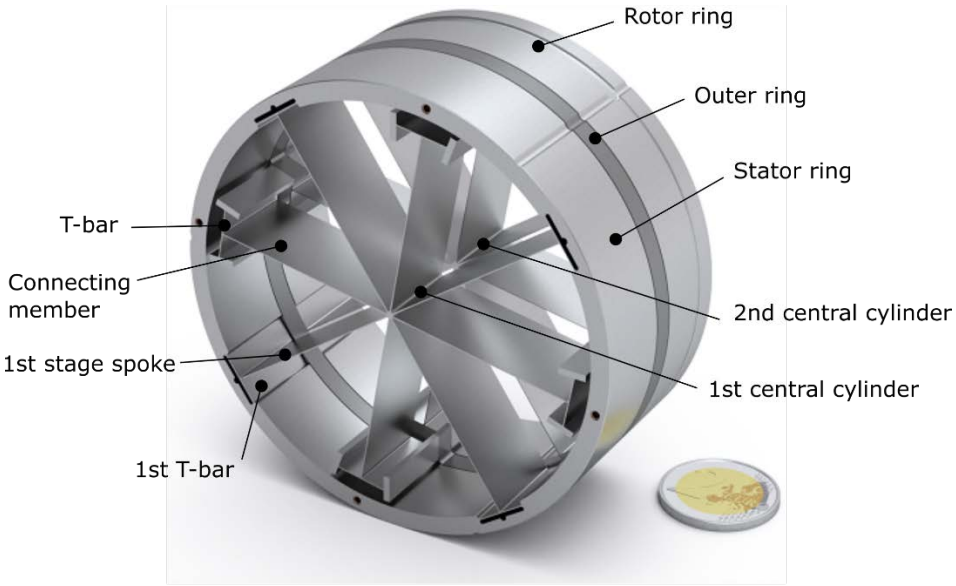

Figure 1. Design Overview of the Almaflex

The number of spokes, connecting members and T-bars can be adjusted to the need of the application. For example, if a larger rotation angle is needed, the blade can be positioned at 120 degrees instead of 90 degrees. The number of spokes and connecting members would thus be 3 instead of 4.

The number of stages can also be increased which will increase the range of rotational angle. The number of thin blades, and spokes can also be increased to raise the torsional stiffness. This is used in oscillating applications to reach high natural rotational eigenfrequencies. All these applications are documented in a world patent[1].

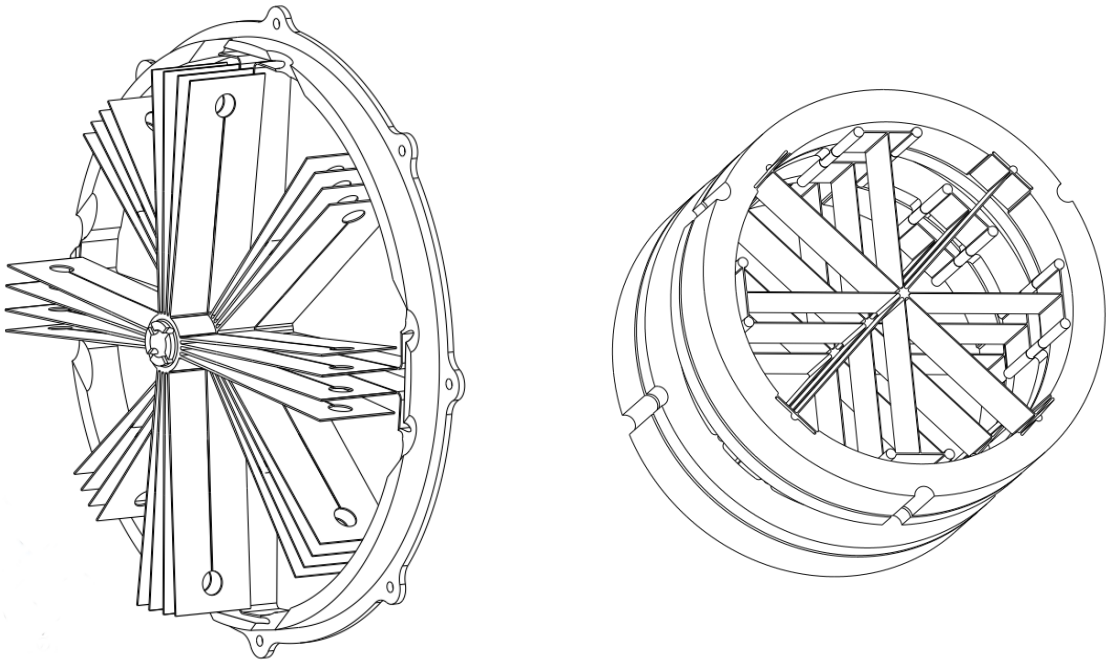

A) B)

Figure 2: A) View of a 3 stage outside-inside design with parallel spokes and connecting members to increase stiffness B) a 3 stage outside-outside design for very large rotational angles.

The advantage of this unique flexible element configuration is that the stiffness in each degree of freedom can be tuned almost independently from the other direction. In particular, the T-bars drive the radial stiffness whereas the total height of the blades drives the axial one. The rotation of the flexure is driven by spokes for approximately one half of the full range while the other half is provided by the connecting members. This decoupling feature is particularly useful for stiffness optimization considering in-orbit operations, launch locking, gravity sag adjustments and can easily be verified via non-linear Finite Element analysis. The fully symmetrical design guarantees no geometrical center shift and, combined with T-bars compliance, a smooth thermo-elastic behavior.

Custom Design for Each Application

The Almaflex design is a family of designs that can be optimized to specific performances. The Large Angle Flexible Pivot (LAFP) is the result of an optimization in response to the European Space Agency (ESA) CTP specifications.

A software tool called FlexOptim has been developed to efficiently find an optimized design within the Almaflex design family that matches best the application requirements.

Rotational angle, applied loads, and launch configuration are given as input to FlexOptim as well as stiffness requirements for radial, axial, torsional and bending cases. The optimization process starts with a baseline set of variables and associated boundaries defining the initial geometry. A set of constants defining material properties and weighting factors are also input. Depending on the configuration during launch: locked or not, a set of design forces is retained for the optimization process. According to the requirements, variables and constants given as input, constraints are generated and cover geometry consistency, targeted stiffness, angle, stress limit and buckling factors. The optimization process starts from the initial set of variables. The optimization process is done in two steps. Optimization loops are performed using analytical formulas that calculate axial, radial, bending and torsional stiffness as well as the stresses and buckling factors. Consistency of these formulas has been correlated with finite element analysis during process development. The optimization aims at minimizing torsional stiffness, volume, and the deviation between targeted and computed rotation angles while maximizing buckling factors and stress performances. In a second step, a complete finite element loop is performed to evaluate the requirements. Correction factors between FE analysis and analytical approach are then computed and considered in the next analytical iterations. The optimal solution is reached when convergence of these correction factors is met. The generic flow logic of the optimization algorithm is shown in Figure 3.

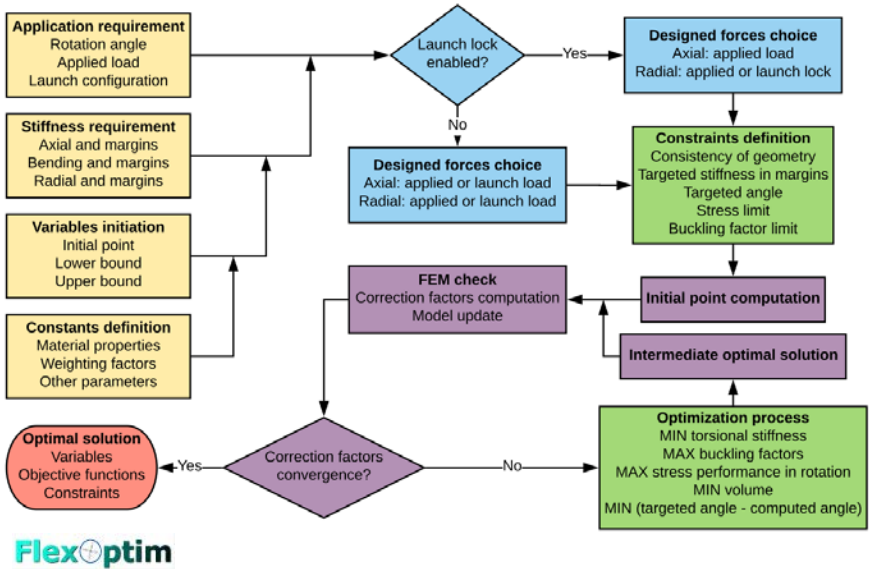

Figure 3: Optimization methodology

Manufacturing constraints are considered by the specification maximal blade length, minimal blade thickness, and allowable range for blade length to height ratio. In addition, specified allowable stress and elastic modulus shall represent achievable values by the end product. To this end, a fatigue test campaign has been set up. Establishment of Wohler curve for titanium grade 5 is currently underway for an ESA CTP project. The preliminary results have shown that the LAFP maximal number of cycles is highly dependent on the manufacturing process (see reference 5 for further details). By selecting the adequate process, 309 million cycles could be achieved without failure. Once the fatigue tests are finished, failure probability analysis will be carried out based on the Wohler curves to identify the maximal safe operation of the LAFP.

The optimization tool used in FlexOptim to minimize or maximize the objective functions is MIDACO[2,3,4] (Mixed Integer Distributed Ant Colony Optimization). MIDACO is a metaheuristic optimizer developed by ESA based on the behavior of ants looking for food around their hill, so its basis of functioning is the exploration of the available space for the variables and the storage of the current best solution. The constraints are handled by using an oracle penalty method. As shown on Figure 4, different levels of exploration can be observed and finally a smaller area around the optimal solution is investigated.

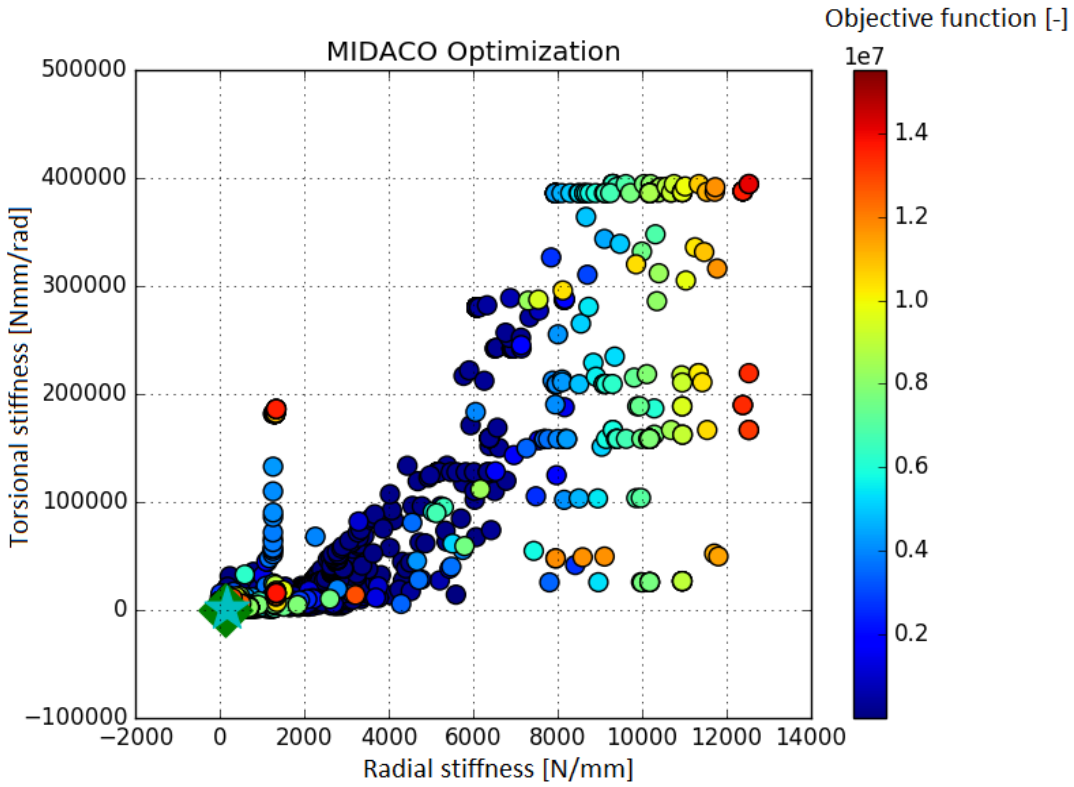

Figure 4: Example of optimization results from MIDACO

Once the optimum geometry fulfils the customer's requirements, the new set of geometry variables are sent automatically to a 3D design software that updates the design.

A Large Family of Designs

Based on the optimization method described above, different designs have been established for a variety of applications. Some of them have been selected to show the different possible design and their main characteristics are shown in Table 1.

Table 1: Main characteristics of some selected applications

Design identification		**D1**	**D2**	**D3**	**D4**
Characteristics	**Unit**				
Application		Pointing	Pointing	Slow Scan	Rapid scan
Payload configuration		Supported on both ends	Supported on both ends	Supported on both ends	Supported on both ends
Launch configuration		Launch lock	Launch lock	Launch lock	Launch lock
Payload mass	kg	2	4	1.2	3.0
Flex material		Titanium	PEEK	Titanium	Stainless Steel
Rotation angle	Degrees	±8.5	±45	±70	±45
Torsional stiffness	Nm/rad	0.33	0.45	0.98	27.3
Axial stiffness	N/m	160000	103000	580000	592000
Radial stiffness	N/m	160000	114000	132000	422000
Radial to torsional stiffness ratio	Rad/m^2	474800	252400	134000	15500
External diameter	mm	47	52	100	172
Overall height	mm	10	23	45	40
Flex mass	kg	0.080	0.027	0.269	0.627

The different designs are shown in the Figure 5.

Design D1

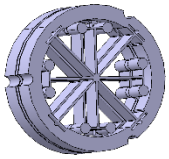

Design D2

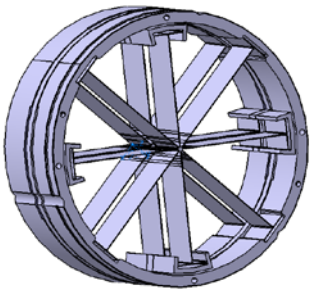

Design D3

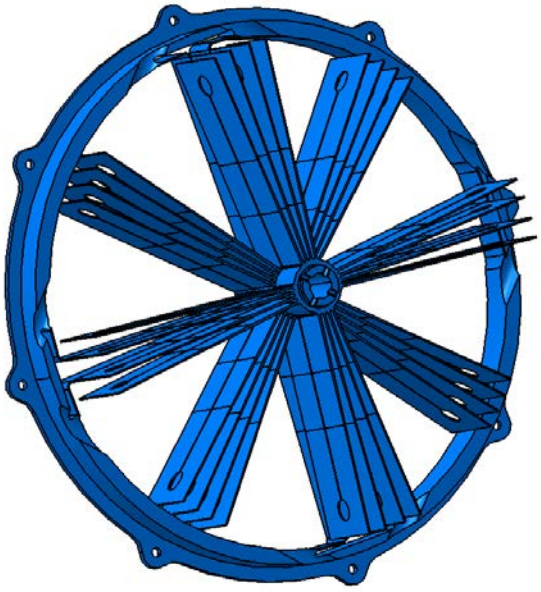

Design D4

Figure 5: Different achievable design listed in Table 1, represented respecting their relative size

PEEK material is used in design D2. This material is very interesting as it is relatively stiff, has good mechanical strength chemical stability, and very good fatigue behavior at the current testing stage. The fatigue stress to Young's modulus ratio, which indicates the ability of a material to deform without fatigue rupture, is 2 to 3 times higher than titanium. A very compact design with large angle is thus achievable, while maintaining high radial to torsional stiffness ratio. In addition, it is very light.

Design D3 is a high-end application for large angle application. The total range of rotational angle is 140 degrees (± 70 degrees), while maintaining lifetime above 100 million cycles with applicable safety margin. The stress and torsional stiffness have been minimized. Center shift is also kept below 10 microns on the entire range of motion. More details on this design can be found in Reference 5.

Design D4 has been developed for a high-frequency oscillatory application that uses the elastic energy as storage. In this application, a cog-free motor is exciting the first torsional mode of the flex with synchronized impulse, which compensates the material damping loss. At each oscillation, the range of motion is increased to reach a maximal oscillation of 90 degrees peak-to-peak (±90 degrees). As the energy stored in the movement is proportional to the flexure's stiffness and to the angular range of motion squared, high stiffness and large angle shall be targeted. In this application, the total elastic energy is 8.4 J per flexure.

It is worth noticing from Table 1 that the LAFP design optimization process is able to achieve very different design goals. For example, in design D1, the application required a relatively small rotational angle. The benefits of the Almaflex design family are the absence of tribological effects thus no wear nor particle generation, and a stable, predictable behavior all-along lifetime. In addition, one unique feature is that the radial stiffness is kept nearly constant during the full rotation. Only 17% stiffness drop is observed between the radial stiffness at 0° rotation and 70°. This feature is essential for micro-vibration isolation.

Micro-Vibration – A Pointing Disturbance

One of the applications of large angle flexible pivot is precision pointing mechanism, such as laser communication terminal, scanner, and flip mirrors. Pointing from a platform to a 1 m diameter target that is distant of 1000 km (Low Earth Orbit) requires a pointing accuracy and stability that is at least a fraction of 1 μrad, typically 0.1 μrad. Such stability requirement may apply to Earth observation satellite, and laser communication between space and ground. For intersatellite laser communication link, the stability requirement is more stringent as the distance between satellites is generally larger, and diameters of target optics are smaller.

To achieve a pointing stability of 0.1 μrad or smaller, understanding the micro-vibration effect on pointing stability is essential. There are sources of vibration noise on each platform. These sources are coming from different moveable parts such as a shutter, solar array drive, reaction wheels, and cryo-coolers. Each of these mechanisms has a micro-vibration signature. Reaction wheels are one of the noisiest equipment. As shown in Figure 6, reaction wheels typically generate low vibration noise at low frequencies and high noise at frequencies above 200 Hz.

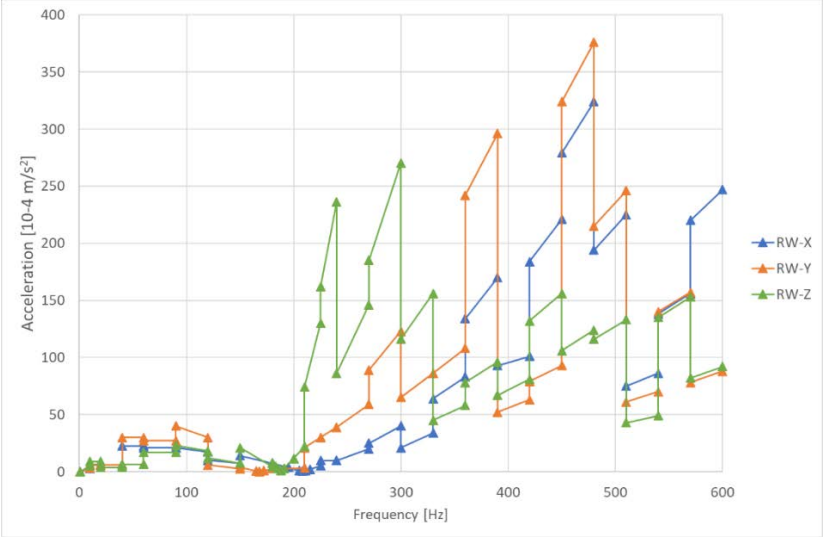

Figure 6: Example of micro-vibration noise specification of reaction wheels for MTG

On the other hand, cryo-coolers generate most of their micro-vibration noise at frequencies around 50 Hz and less at higher frequencies. Note that the level of micro-vibration from cryo-coolers is generally smaller than those of reaction wheels, even at 50 Hz.

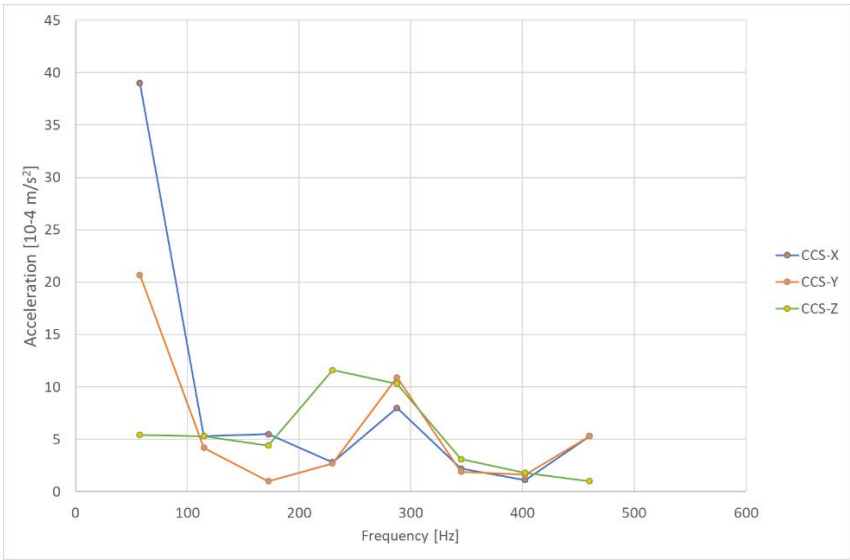

Figure 7: Example of micro-vibration noise spectrum for cryo-coolers on MTG

The different sources of micro-vibration add up at the pointing mechanism interface. The micro-vibrations are then transmitted to the mirror by the pointing mechanism which disturb the pointing stability. Translation vibration of the mirror are generally not a concern as it does not affect pointing stability. On the other hand, rotational vibration of the mirror has a direct effect on the pointing stability. The transfer function between the pointing mirror and the pointing mechanism's interface to the spacecraft is thus key.

In case of a stiff pointing mechanism using ball bearings, the structure transfer function has a first amplification peak at its first structural eigenfrequency, which is typically between 140 Hz for spacecraft decoupling requirement and below 1000 Hz. Below the first eigenfrequency, micro-vibrations are either transmitted to the mirror integrally for frequencies far below the peak or amplified for the ones near

resonance. Thus, cryo-coolers micro-vibrations that have the highest excitation at frequencies between 50 and 100 Hz are integrally transmitted to the pointing mirror. In addition, high level micro-vibration noise from reaction wheels may well coincide with the first structural eigenmode of the pointing mechanism, leading to huge amplification. The first eigenfrequency of the pointing mechanism shall thus be tuned to match the reaction wheels quiet area.

To illustrate this phenomenon on a classical series azimuth-elevation pointing mechanism, a simplified Nastran model was built (see Figure 8).

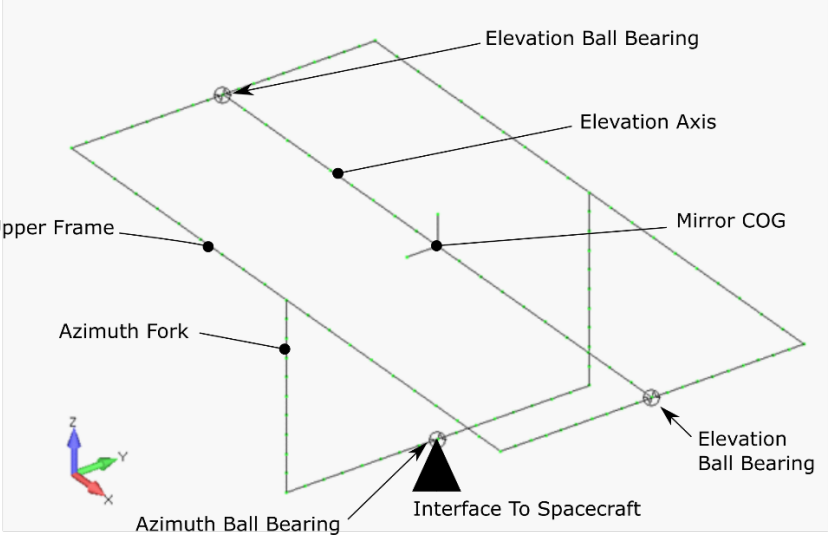

Figure 8: Description of the simplified Nastran model

The interface of the mechanism to the spacecraft is modeled by a single node and a CBUSH element. The CBUSH has the stiffness properties of the azimuth ball bearing with low rotational stiffness around Z axis. The azimuth fork connects the azimuth ball bearing to the upper frame. The elevation axis is connected to the upper frame by two CBUSHs representing the elevation axis ball bearings. The mirror CoG is located at the intersection of the azimuth and elevation axis.

The beam section has been tuned to obtain a first frequency above 140 Hz, and near the quiet reaction wheel zone that is below 200 Hz and the CBUSH spring constant has been chosen to represent ball bearings stiffness. The total mass of the modeled mechanism is about 7 kg.

The eigenfrequencies and modal effective mass of the simplified model of a pointing mechanism using ball bearing is shown in Table 2. The participating mass and inertia that are dominant for each mode has been highlighted in Table 2.

Table 2: Ball bearing pointing mechanism eigenfrequencies and participating mass

ID	Freq	TX	TY	TZ	RX	RY	RZ
	Hz	kg	kg	kg	kg m^2	kg m^2	kg m^2
1	0.2	-2.74E-05	-1.33E-05	1.95E-16	1.10E-08	1.46E-10	**-2.13E-01**
2	4.3	1.62E-15	-3.55E-05	-8.11E-10	**.521E-01**	-2.45E-17	-.116E-12
3	163.4	-3.29E-10	**2.59E+00**	.278E-05	-4.09E-03	-.242E-10	-2.54E-12
4	179.9	**1.15E+00**	3.98E-10	-2.81E-05	1.23E-11	**1.68E-01**	-1.78E-12
5	499.6	**-2.33E+00**	6.44E-12	-2.46E-05	2.31E-11	**.845E-01**	.544E-12
6	779.9	-.974E-05	-1.54E-05	**2.57E+00**	-1.54E-05	1.51E-06	9.89E-18

The first two modes are the ones associated with the azimuth and elevation rotation axes. As these modes are controlled by the elevation and azimuth motors, they are not a concern in the micro-vibration analysis. The 3rd mode is a translational mode in Y direction and takes place at 163 Hz. The 4th and 5th modes are due to the bending of the azimuth fork and combine a translation in X and a rotation around Y. Finally, the 6th mode is a translational mode in Z direction.

A frequency response (SOL111) analysis is carried out with a unit acceleration excitation in each translational and rotational direction. The X, Y, Z displacements and angles of the mirror center of gravity are monitored giving 36 transfer functions of the mechanism. The responses that are the most detrimental to the pointing stability are the Y rotation (elevation) due to X-translation excitation, and Y rotation due to Y-rotation excitation (see Figure 9).

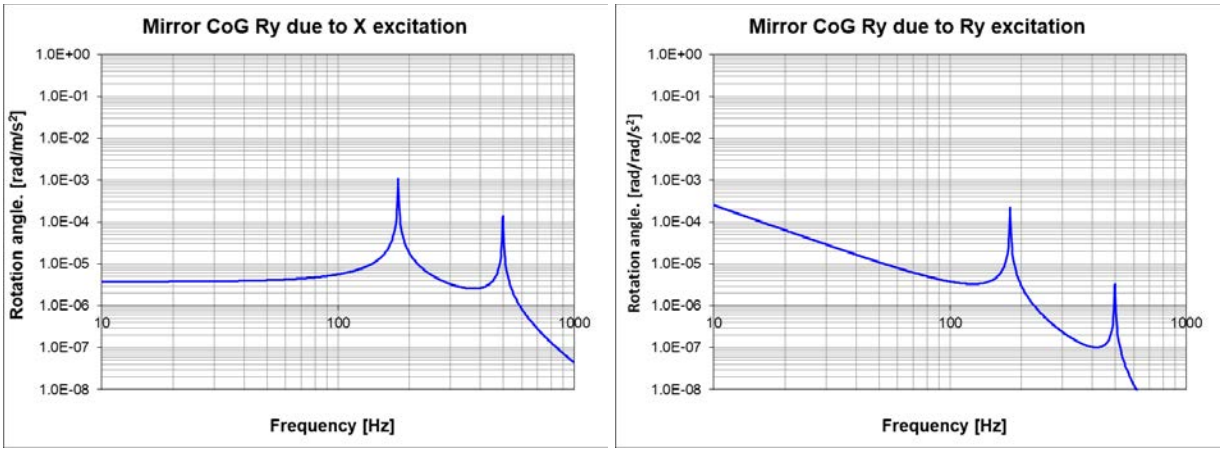

Figure 9: Ball bearing pointing mechanism response on elevation axis rotation (Y-rotation) for a X-translational (left) and a Y-rotational (right) unit acceleration excitation

Figure 9 shows that even though the mirror is perfectly balanced, micro-vibration at the base of a stiff pointing mechanism will be amplified by the structural mode and lead to rotation of the mirror around elevation axis. These perturbations cannot be compensated by drive electronics as they are taking place above the control frequency bandwidth. In addition, the prediction of the induced movement can be difficult, as the mode shape is playing a key role. In an optimistic approach, where the mirror is perfectly balanced and the first main mode located in a rather quiet micro-vibration frequency range where acceleration is 0.001 m/s^2, the micro-vibration-induced motion around the elevation axis is on the order of 1 μrad for X translation excitation. On top of this, the motion due to Y rotation excitation shall be added as well as all the noise coming from the mechanism ball bearings and the induced motion from unbalanced mass. In these conditions, it is difficult to reach the stability requirement of 0.1 μrad or smaller.

Passive Damping of Micro-vibration

A simple way to reduce the micro-vibration effects on the mirror pointing stability is to introduce compliance in the system. The goal is to control and lower the rotational eigenfrequencies of the pointing mechanism below micro-vibration excitation frequencies from the spacecraft but still above control loop frequencies. A pointing mechanism with such low resonance frequency is passively damping the micro-vibration thanks to the natural transfer function decay observed above resonance frequency.

Compliance is efficiently introduced in the mechanism using flexible pivots. A novel concept of a pointing mechanism has been developed to cover a full hemispherical pointing range. A fully functional, and motorized breadboard has been built to verify the functional and range requirement and is shown in Figure 10. The beauty of this concept is that it replaces the traditional coarse and fine pointing mechanism

used in high accuracy pointing mechanisms by one unique ultra-stable pointing mechanism with micro-vibration isolation capability, bringing mass, volume and cost down.

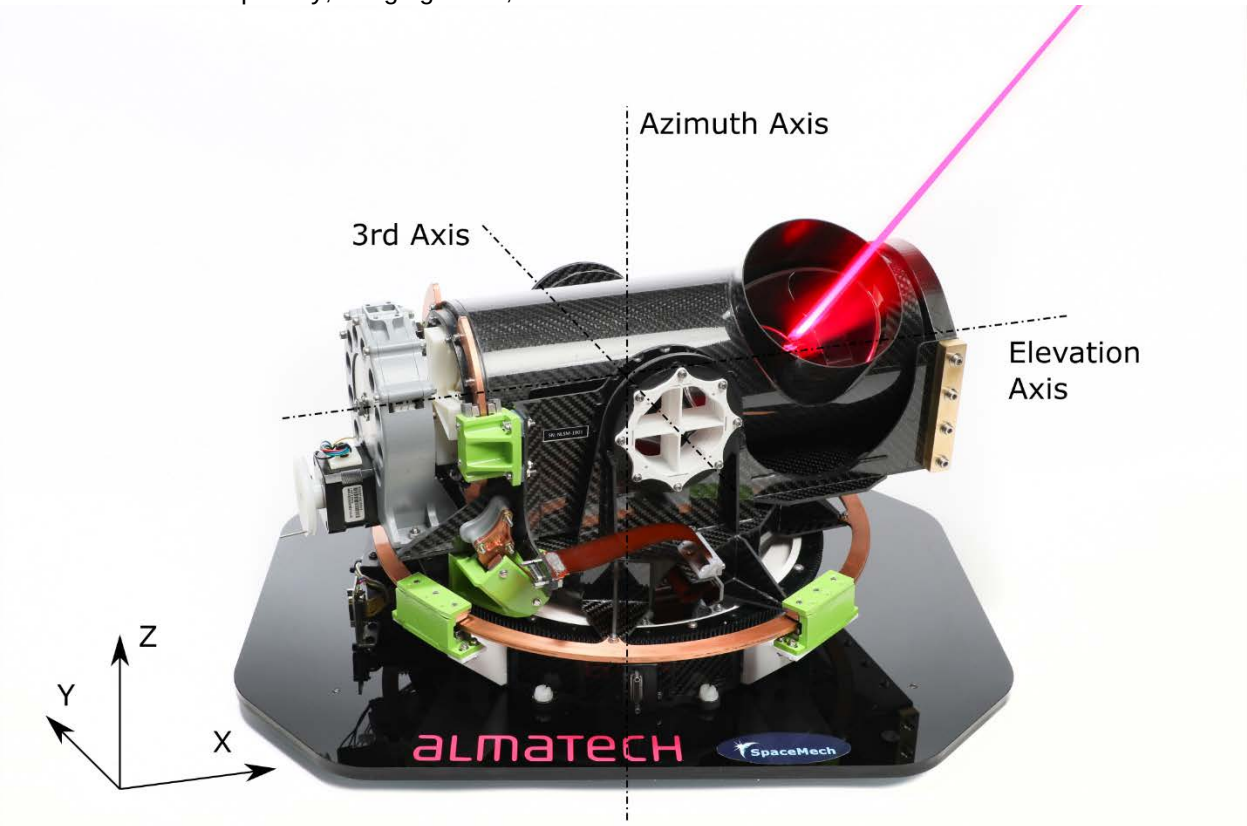

Figure 10: Novel concept of pointing mechanism

The pointing mirror is supported by two large angle flexible pivots similar to the D3 design presented earlier and provides the elevation rotation around X. Their stators are connected to a frame structure by two small angle flexible pivots (3rd Axis) to lower the Y rotation eigenmode of the elevation axis. The stator side of the small angle 3rd axis pivots is then connected to the azimuth fork. The azimuth fork is then connected to the azimuth ball bearing by a set of small angle flexible structures for decoupling the azimuth rotation axis from azimuth motorization mode, azimuth ball bearing, and spacecraft-born rotational micro-vibration. A flexible pivot is used between the elevation stepper and elevation axis to filter out the high frequency micro-vibration noise coming from the motor.

The novel pointing mechanism dynamic behavior is studied using a simplified Nastran model shown in Figure 11.

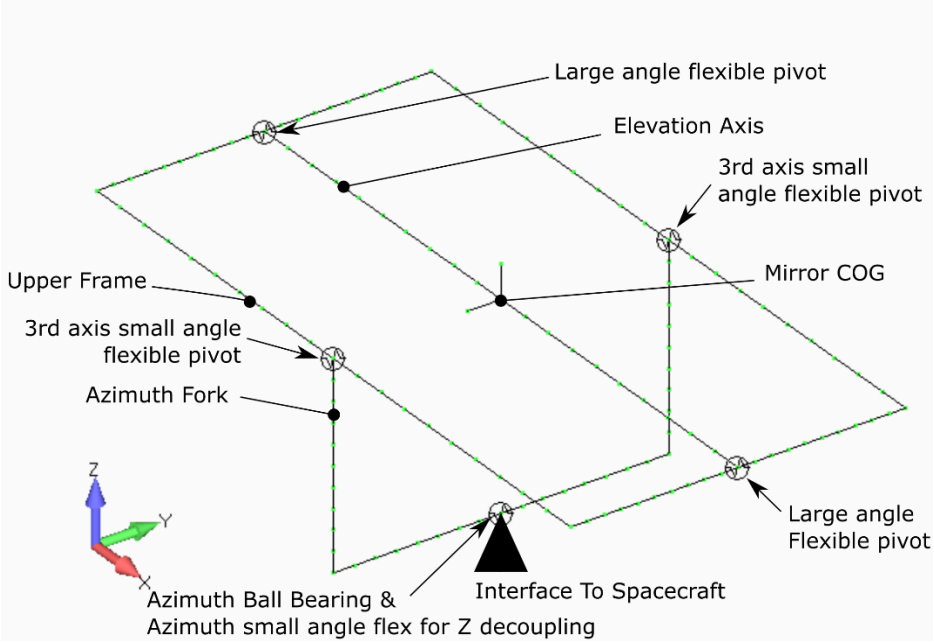

Figure 11: Simplified Nastran model of the novel pointing mechanism

The exact same structural properties have been used for the novel concept using flexible pivots as in the ball bearing version presented previously. The notable difference is that the axial, radial, bending and torsional stiffness of the flexible connection have been tuned to lower the first eigenmodes. Table 3 shows the eigenfrequencies of the first 12 modes together with their participating mass and inertia.

Table 3: Novel concept pointing mechanism using flexible pivots eigenfrequencies and participating mass

ID	Freq	TX	TY	TZ	RX	RY	RZ
	Hz	kg	kg	kg	kg m^2	kg m^2	kg m^2
1	0.2	7.51E-10	1.78E-10	8.90E-29	1.21E-16	1.52E-20	**4.53E-02**
2	0.4	1.90E-11	2.13E-27	2.41E-10	2.62E-28	**3.53E-02**	7.38E-22
3	4.3	2.76E-28	1.28E-09	6.58E-19	**.272E-02**	3.35E-27	3.73E-26
4	20.6	7.84E-25	**1.22E+00**	1.51E-16	6.98E-10	5.15E-29	5.45E-25
5	20.6	1.01E-15	2.92E-17	**1.19E+00**	3.55E-19	7.84E-23	5.34E-30
6	29.2	**1.20E+00**	3.56E-25	1.16E-15	2.19E-27	6.93E-12	2.24E-25
7	46.9	7.46E-11	1.96E-11	1.71E-25	1.64E-17	9.07E-21	2.82E-12
8	47.6	3.96E-12	2.01E-28	3.08E-11	4.42E-28	1.81E-11	7.78E-31
9	180.6	5.94E-20	**5.47E+00**	9.60E-12	2.09E-05	5.75E-28	2.96E-24
10	362.4	**5.51E+00**	9.92E-21	2.97E-10	5.12E-22	6.80E-07	1.35E-24
11	839.4	2.97E-17	1.26E-02	5.11E-07	**1.34E-02**	7.56E-24	1.03E-24
12	870.8	3.06E-10	9.74E-10	**5.44E+00**	1.08E-09	8.22E-17	7.64E-32

Modes number 1 and 3 are the same ones as those of Table 2, and are rotational modes around azimuth and elevation axes. Mode number 2 is a new mode introduced by the 3rd axis which will greatly help to damp Y rotations of the mirror under perturbations coming from the spacecraft interface.

Modes 4, 5 and 6 are translational modes of the elevation axis. Thanks to the low radial and axial stiffness of the large-angle flexible pivot, it is possible to lower these modes below the excitation frequencies of cryo-coolers while keeping them well above typical controller frequency and avoid control issues.

Modes 7 and 8 are rotational modes of the elevation axis around the mirror CoG. Modes 9, 10 and 12 are translation modes of the azimuth fork and upper frame combined. Benefits of decoupling the elevation axis from the rest of the structure can already be observed by looking at the participating mass. Indeed, the participating mass of these modes is close to the total mass minus the mass of the elevation axis.

A frequency response analysis (SOL111) is performed with unit acceleration excitations at the mechanism interface with the spacecraft. The transfer functions between mirror CoG motion and excitation are calculated and compared to the ones obtained with the ball bearings model. In all cases, significantly lower responses are observed. To illustrate this, the two transfer functions shown in Figure 9 are reproduced in Figure 12 together with the ones obtained with the flexible pivots concept.

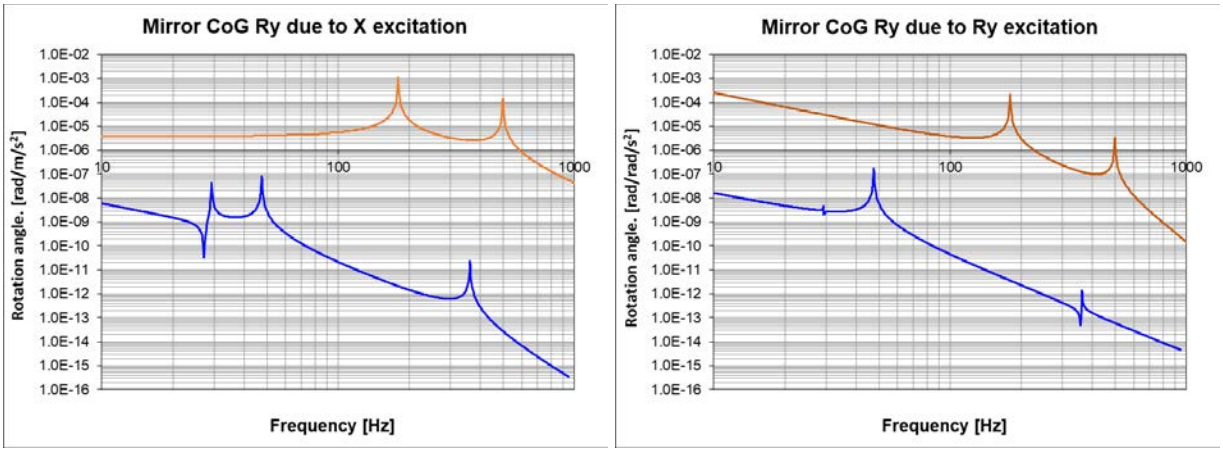

Figure 12: Flexible pivots pointing mechanism response (in blue) and ball bearings mechanism (in red) on elevation axis (Y-rotation) for X-translational (left) and Y-rotational (right) unit acceleration excitation

The transfer functions show strong attenuation of the micro-vibration. Most of the peaks are located in the 10 to 50 Hz bandwidth which is outside of typical micro-vibration spectrums. In the bandwidth between 50 and 200 Hz corresponding to intermediate micro-vibration excitation from cryo-cooler and reaction wheels of 0.001 m/s^2, the maximal mirror rotation around Y is 6E-6 μrad at 47Hz, 6E-7 μrad at 50 Hz, and 3E-9 μrad at 200 Hz. Note that these values are for Ry excitation and are smaller for X excitation. The stability of a compliant pointing mechanism is thus between 3 and 8 orders of magnitude better than classical ball bearing pointing mechanism.

To further improve pointing stability, dampers are added on the elevation, azimuth and 3rd axis. These dampers are acting in rotation but also in radial directions. The effect of these dampers decreases the local amplification at resonance peak. The elevation rotation due to X excitation can be reduce by a factor 5 on the mode at 29 Hz and by a factor of 10 for the mode at 49 Hz.

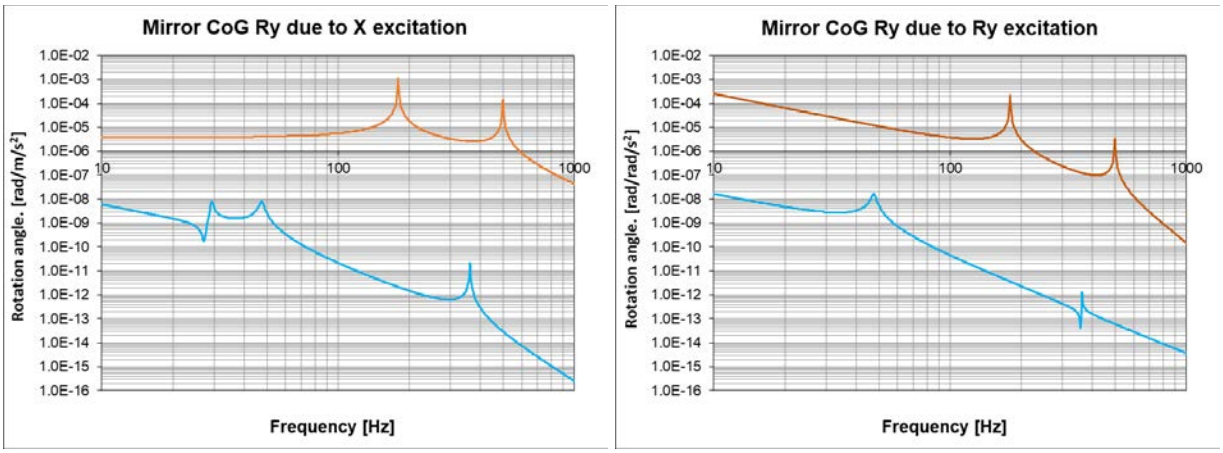

Figure 13: Flexible pivot pointing mechanism response with dampers (in light blue) and with ball bearing (in red) on elevation axis (Y-rotation) for a X-translational (left) and a Y-rotational (right) unit acceleration excitation

Conclusion

The development of a novel, highly customizable flexible pivot is opening new design possibilities. Thanks to a fully automatized optimization software, it is possible to design within a few hours a tailor-made flexible pivot that matches specific stiffness, range of motion, and lifetime requirements. In addition, it is possible to cover a wide range of requirements, from low torsional to high torsional stiffness and from high to low torsion to radial stiffness. The application of flexible pivots is thus numerous, from high-precision pointing mechanisms, to infinite-life oscillation scanner or to energy storage applications.

By combining large-angle and small-angle flexible pivots, micro-vibration excitation can be ruled out from the pointing accuracy budget. It is shown that it is possible to lower the micro-vibration impact on the pointing stability by 3 to 8 orders of magnitude between 50 to 200 Hz by the introduction of compliance at strategic locations. In the frequency range above 200 Hz, which is the noisiest bandwidth of reaction wheels, such a novel concept is bringing the level of perturbation angle below 5E-10 rad/m/s^2.

The addition of dampers on the three axes can further improve the pointing stability by a factor of 5 to 10 in comparison to the pointing mechanism using flexible pivots alone. It is thus possible to replace the combination of coarse and fine pointing mechanisms by a single mechanism achieving ultra-stable pointing stability. The total mass of the system can be drastically reduced, as well as the total volume. Finally, the novel ultra-stable pointing mechanism using flexible pivots is very cost effective in comparison to solutions available today on the market. The highly customizable flexible pivot design family is an enabling technology for many applications such as ultra-high precision pointing mechanisms.

References

1. L. Blecha, M. Humphries, Y. Puyol, WO2017077469A1
2. Schlüter, M. &. (2010). The oracle penalty method. In Journal of Global Optimization, 47(2) (pp. 293-325).
3. Schlüter, M. E. (2009). Extended ant colony optimization for non-convex mixed integer nonlinear programming. In Computers & Operations Research, 36(7) (pp. 2217-2229).
4. Schlüter, M. G. (2012). A numerical study of MIDACO on 100 MINLP benchmarks. In Optimization, 61(7) (pp. 873-900).
5. Puyol, Y. (2019). Innovation in Large angle flexible pivot Design & Material Accelerated Fatigue Screening Tests Results. In ESMATS 2019.